






Article

Development of an Optimized Non-Linear Model for Precise Dew Point Estimation in Variable Environmental Conditions

José Antonio Hernandez-Torres ¹, Juan P. Torreglosa ^{1,*}, Reyes Sanchez-Herrera ¹, Aldo Bischi ²
and Andrea Baccioli ²

¹ Department of Electrical, Thermal, Design and Projects Engineering, Escuela Técnica Superior de Ingeniería, Universidad de Huelva, Avda. de las Fuerzas Armadas s/n, 21007 Huelva, Spain; joseantonio.hernandez@dimme.uhu.es (J.A.H.-T.); reyes.sanchez@dfaie.uhu.es (R.S.-H.)

² Department of Energy, Systems, Territory and Construction, DESTEC, Università di Pisa, Via Carlo Francesco Gabba 22, 56122 Pisa, Italy; aldo.bischi@unipi.it (A.B.); andrea.baccioli@unipi.it (A.B.)

* Correspondence: juan.perez@die.uhu.es

Featured Application: Studies utilizing GIS-based tools (e.g., PVGIS), which provide localized atmospheric data with a limited number of parameters.

Abstract: Accurate dew point estimation is crucial for measuring water condensation in various fields such as environmental studies, agronomy, or water harvesting, among others. Despite the numerous models and equations developed over time, including empirical and machine learning approaches, they often involve trade-offs between accuracy, simplicity, and computational cost. A major limitation of the current approaches is the lack of balance among these three factors, limiting their practical applications under diverse conditions. This research addresses these key challenges by developing a new, streamlined equation for dew point estimation. Using the Magnus–Tetens equation, deemed as the most reliable equation, as a benchmark, and by applying a process of non-linear regression fitting and parametric optimization, a new equation was derived. The results demonstrate high accuracy with a streamlined implementation, validated through extensive data and computational simulations. This study highlights the importance of accurate dew point modeling, especially under variable environmental conditions, provides a reliable solution to existing limitations, paving the way for enhanced efficiency in related processes and research endeavors, and offers researchers and practitioners a practical tool for more effective modeling of water condensation phenomena.

Keywords: dew point estimation; water condensation modeling; parametric optimization



Citation: Hernandez-Torres, J.A.; Torreglosa, J.P.; Sanchez-Herrera, R.; Bischi, A.; Baccioli, A. Development of an Optimized Non-Linear Model for Precise Dew Point Estimation in Variable Environmental Conditions. *Appl. Sci.* **2024**, *14*, 10508. <https://doi.org/10.3390/app142210508>

Academic Editor: Jane J. Liu

Received: 4 September 2024

Revised: 31 October 2024

Accepted: 12 November 2024

Published: 14 November 2024



Copyright: © 2024 by the authors. Licensee MDPI, Basel, Switzerland. This article is an open access article distributed under the terms and conditions of the Creative Commons Attribution (CC BY) license (<https://creativecommons.org/licenses/by/4.0/>).

1. Introduction

1.1. State of the Art

The accurate estimation of dew point temperature (DPT) plays a crucial role in enhancing the efficiency and performance of various systems, ranging from meteorological forecasting to industrial applications, extending to the design of atmospheric water capture systems [1,2]. The DPT refers to the temperature at which the atmosphere reaches saturation with water vapor, leading to the condensation of a portion of this suspended water [3]. The DPT is invariably lower than or equal to the ambient temperature. Consequently, precise determination of the DPT holds significant importance, as it governs heat stress on individuals, and monitors variations in evaporation rates and humidity trends [4].

Beyond its fundamental thermodynamic relevance, the dew point serves as a connection between theoretical understanding and practical applications across diverse fields such as agriculture, horticulture, and agronomy, where seasonal DPT trends inform irrigation strategies and optimize water usage, maximizing crop productivity [5]. Additionally, accurate weather pattern prediction relies on incorporating DPT calculation into models,

providing insights for public safety, agricultural planning, and climate research [6]. Furthermore, DPT plays a crucial role in various engineering applications such as construction [7,8] and industry. Controlling humidity through dew point manipulation is essential for ensuring product quality and process efficiency in diverse sectors like food processing [9], electronics manufacturing [10], or water harvesting [2,11]. Additionally, most studies analyzing humid air in ambient conditions of temperature and pressure focus on partial pressure calculation, relegating the DPT as a secondary parameter [12,13]. Nevertheless, the dew point is a key factor for different fields, especially, but not limited to, water harvesting, where cooling the air below its DPT consumes enormous energy and causes low energy efficiency, especially in hot and dry areas [14].

Regarding the specific DPT calculation, various methods for determining the DPT have been discussed, including empirical equations, depending on the operating conditions. Different correlations have been developed to determine properties of compressed humid air [15–17]. To date, the estimation of DPT in ambient conditions was traditionally performed using empirical equations [18]. In this regard, among the most common approaches, the rule of thumb for moist air suggests a 1 °C decrease in DPT for every 5% decrease in relative humidity, starting at the dry bulb temperature when RH = 100% [19]. However, these methods are limited in their accuracy, particularly under varied environmental conditions, including the spectrum of average conditions of temperature and humidity, but also very high temperatures (above 40 °C) or temperatures near 0 °C, where condensation becomes challenging. Additionally, conditions of very high relative humidity (above 80%) and very low relative humidity (below 15%) further complicate the accuracy. Combining extreme temperatures with extreme humidity levels presents the most difficult scenarios for accurately modeling the DPT.

With the development of Machine Learning and Soft Computing Techniques (SCTs), more sophisticated models have been developed for DPT estimation. Support Vector Regression (SVR), optimized with algorithms such as Ant Colony Optimization (ACO), has been employed to balance accuracy and complexity, providing DPT estimations across different climatic conditions [20,21]. Artificial Neural Networks (ANNs) and Adaptive Neuro-Fuzzy Inference Systems (ANFISs) have shown great potential in capturing non-linear relationships between meteorological variables and DPT. Studies have demonstrated their effectiveness, particularly when integrated with optimization techniques like Genetic Algorithms (GAs) [22,23]. Likewise, hybrid models, which combine different computational techniques, are also employed, enhancing the accuracy of DPT estimation [21]. Additionally, studies have shown that integrating Genetic Algorithms (GAs) to optimize the parameters of Least Square Support Vector Machine (LSSVM) and ANFIS can significantly improve the predictive performance, making these models valuable tools for practical applications [24].

While these previous works [16–27] discuss methods and approximations, there are no specific equations or models using only ambient temperature and relative humidity as single inputs for calculating water DPT. Furthermore, soft computing models do not explicitly reveal the correlation between input and output data, making it difficult to understand the relationships and reasoning processes. In contrast, mathematical approaches or physical-based equations provide clear and explicit correlations between inputs and outputs, offering a transparent justification of the results. While SCT models are effective, their lack of interpretability can be a significant drawback in applications requiring clear understanding and justification of the predictions [25].

Late studies exploring hybrid SCTs highlight the importance of minimizing computational demands while maintaining high accuracy, which is crucial for practical applications [26,27]. Computational demand refers to the amount of resources, such as processing time and memory, required to perform a task. Simplifying an equation does not significantly reduce computational load on modern processors, but simplicity can enhance usability and reduce the risk of errors. For instance, adding a single mathematical operation may have a minimal effect on a one-time calculation, but can significantly increase the load depending on the type of operation and the ongoing process. Considering addition/subtraction as

the elemental baseline of computing, taking around 1 ns per operation, other operations require more time: multiplication takes 5–10 times more, division 10–20 times more, exponentiation 20–30 times more for small exponents (and much higher for large exponents), square roots 30–40 times more, logarithms 50–100 times more, and trigonometric functions 100–200 times more. These differences are further influenced by the specific algorithms and implementation strategies used in software and platforms, with efficient algorithms significantly enhancing performance [28,29]. Furthermore, iterative calculations, optimization problems, and especially nested operations can repeat these operations dozens to thousands of times. Using RAM for storing intermediate results offers the fastest access with times in the order of nanoseconds to microseconds. However, this approach can be constrained by the available memory, particularly for large-scale computations, where writing results to temporary files can introduce considerable overhead, increasing access times to milliseconds, which is approximately 1000 times slower [30]. Therefore, reducing and replacing operations correctly can significantly reduce computing time. Recent works have emphasized that developing new, accurate, and reliable dew point equations for scientific and practical applications would contribute to applied thermal engineering and energy-efficient system designs [21].

1.2. Research Gaps

Despite advancements in DPT estimation models, several gaps persist in the existing literature, limiting the effectiveness and applicability of these models in various scenarios:

- **Dependence on Multiple Variables:** Many models require different meteorological variables (e.g., temperature, humidity ratios, vapor pressure), complicating their use and implementation. Simplifying the input requirements can make models more accessible and easier to implement, especially in resource-constrained environments [16–27].
- **Limited Applicability under Varied Conditions:** These conditions include the spectrum of average conditions of temperature and humidity, but also very high temperatures (above 40 °C) or temperatures near 0 °C, where condensation becomes challenging. Additionally, conditions of very high relative humidity (above 80%) and very low relative humidity (below 15%) further complicate the accuracy. Combining extreme temperatures with extreme humidity levels presents the most difficult scenarios for accurately modeling the DPT. Current empirical models and some machine learning models fail to provide accurate estimates under extreme environmental conditions. Accurate DPT estimation under a wide range of conditions is critical for applications like water harvesting and energy efficiency [8,9,15,27,28].
- **Lack of Specialized Tools:** Currently, there is no tool specifically designed to address the combined results of temperature and humidity conditions beyond the simplistic rule of thumb, which is often inadequate. Developing dedicated tools that can handle these combined scenarios with precision and reliability is essential for advancing practical applications and enhancing model accuracy in diverse environmental contexts.

1.3. Contributions

This study aims to address these identified research gaps by developing a new, simplified, and accurate dew point estimation equation based solely on ambient temperature and relative humidity. In this regard, this work provides the following contributions:

- **Development of a specific equation:** This work introduces a new equation obtained through non-linear regression fitting and parametric optimization, using only ambient temperature and relative humidity. This simplifies the input requirements while maintaining high accuracy, making the model more practical and accessible. This work provides a robust tool for optimizing water harvesting and other related processes, improving overall efficiency.
- **Enhanced accuracy across conditions:** The equation is validated through extensive data comparison, demonstrating consistent accuracy under real environmental conditions.

This ensures reliable performance in critical applications, especially in hot and dry areas where energy efficiency is paramount.

- An equation which is particularly useful for environmental studies: This work utilizes GIS-based tools (e.g., PVGIS), which provide localized atmospheric data with a limited number of parameters. Having a model dependent on as few parameters as possible is crucial for its applicability and real-world implementation.

By addressing these gaps, this study offers a practical and reliable solution for DPT estimation, benefiting both scientific research and practical applications. For this purpose, this paper is organized as follows: Section 2 presents a comprehensive literature review identifying research gaps, establishing precise research objectives, and clarifying the paper's contributions. Subsequently, a description of the methodological process followed are presented in Section 3. The obtained equations are presented, analyzed, and evaluated in Section 4. Finally, Section 5 presents the conclusions of the research.

2. Materials and Methods

2.1. Background

The estimation of DPT in ambient conditions traditionally relies on empirical equations [18], but there are also theoretical ones. Among the most common approaches for humid air conditions, the rule of thumb suggests a 1 °C decrease in DPT for every 5% decrease in relative humidity, starting at the dry bulb temperature when RH = 100%, as indicated in Equation (1) [19]. Furthermore, the most relevant empirical equations are the Buck's equation [31], Goff–Gratch's equation [32], and Magnus–Tetens' equation [33].

$$DPT = T - \frac{100 - RH}{5} \quad (1)$$

where:

- T refers to the ambient temperature,
- RH corresponds to the relative humidity of the air.

Magnus–Teten's equation, described in Equation (2):

$$DPT = \frac{273.3 \times \left(\ln\left(\frac{17.269}{RH}\right) + \frac{17.269 \times T}{237.3 + T} \right)}{17.269 - \left(\ln\left(\frac{17.269}{RH}\right) + \frac{17.269 \times T}{237.3 + T} \right)} \quad (2)$$

where:

- T refers to the ambient temperature,
- RH corresponds to the relative humidity of the air,
- 273.3 and 17.269 are non-dimensional coefficients.

Regarding theoretical equations, the most relevant one is the Clausius–Clapeyron equation [34], described in Equation (3):

$$DPT = T \left[1 - \frac{T \cdot \ln\left(\frac{RH}{100}\right)}{L/R_w} \right]^{-1} \quad (3)$$

where:

- $T = 273.15$ K,
- L is the enthalpy of vaporization; $L = 2.501 \times 10^6 \frac{\text{J}}{\text{kg}}$ ($T = 273.15\text{K}$) \div $2.257 \times 10^6 \frac{\text{J}}{\text{kg}}$ ($T = 373.15\text{K}$),
- R_w is the gas constant for water vapor; $R_w = 461.5 \frac{\text{J}}{\text{K}\cdot\text{kg}}$.

Equation (3) gives a good approximation to Magnus–Tetens' equation (Equation (2)) when T is close to the value for which L is chosen, with small but non-negligible errors away from the chosen reference temperature.

The most commonly used equation to obtain the DPT based on the ambient temperature and relative humidity is the previously defined rule of thumb. Previous works delve into the mathematical basis and accuracy of different relationships between dew point and relative humidity, presenting practical applications like computing the cumulus cloud-base level. However, the exact conversion from relative humidity to DPT is complex. One of the main problems highlighted is the difficulty in achieving highly accurate approximations without sophisticated tools, emphasizing the need for simpler yet reliable methods for practical applications in meteorology and atmospheric science [4]. Based on this, the most common problems associated with existing dew point equations based on temperature and relative humidity include:

- Complexity: Many existing equations for calculating dew point from temperature and relative humidity are complex and demand a higher computation cost, especially in case of iterative calculations.
- Accuracy: Some equations may lack accuracy, especially in approximating the conversion from relative humidity to DPT, leading to potential errors in moisture content estimations in the air.
- Pressure dependency: The accuracy of dew point calculations can be influenced by variations in pressure, affecting the reliability of the results, especially in scenarios where environmental conditions fluctuate significantly. Additionally, it supposes an additional variable to consider while solving the defined problem.

Addressing these common issues in dew point equations is essential to improve the accuracy, simplicity, and reliability of calculations related to DPT and relative humidity in atmospheric science and meteorology.

2.2. Problem Definition and Methodology

The objective is to estimate the DPT using just ambient temperature and relative humidity. To address this problem, mathematical models derived from empirical data are used. By leveraging upon known relationships between temperature, humidity, and dew point, it is possible to construct equations that approximate the DPT based on ambient conditions. These equations are formulated through non-linear regression fitting and parametric optimization and the subsequent validation processes, ensuring their reliability and accuracy across various scenarios.

Following the development of these equations, their efficacy is assessed through established statistical measures, quantifying the correspondence between forecasted and observed DPT. This systematic approach's workflow is shown in Figure 1. The observed data constitutes a dataset utilized for dual purposes: as training and testing data. The training dataset serves as the foundation for deriving equations that model the data distribution. Should the obtained equations yield satisfactory results ($R^2 > 0.95$, $STD < 2$), the process proceeds to optimization; otherwise, it reverts to mathematical modeling. Subsequent to the optimization phase, where the coefficients are tuned, the results undergo statistical scrutiny to ascertain any enhancements compared to prior iterations. Specifically, an approximation target of $R^2 \geq 0.99$ and $STD < 1$ is sought. Subsequently, an iterative simplification procedure ensues, wherein the decimal precision of equation components is successively reduced. Acceptance of modifications is contingent upon the demonstration of improved results after each iteration; otherwise, iterations are performed on a term-by-term basis of the equation. Should any variation yield superior outcomes, the process concludes.

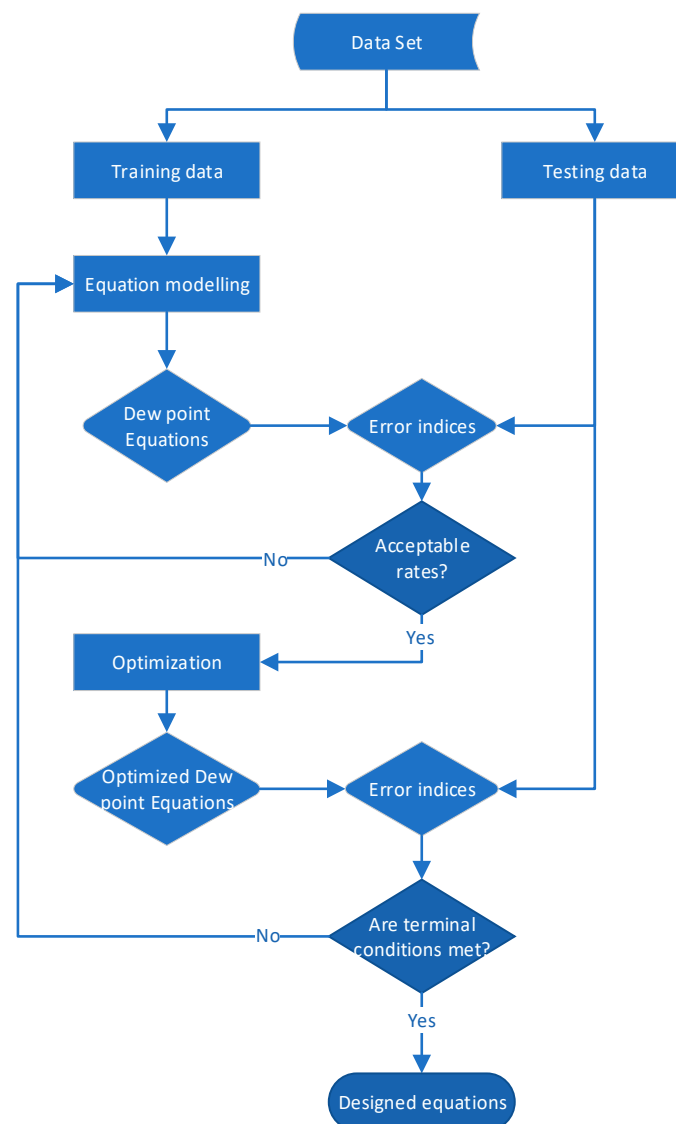


Figure 1. Workflow diagram of the modeling, optimization, and testing process.

2.3. Equation Finding

2.3.1. Preliminary Considerations

The computational cost of an equation refers to the amount of computational resources required to solve it. This cost is typically measured in terms of: (1) time complexity, i.e., the number of elementary operations needed to solve the equation as a function of the input size (number of variables, terms); and (2) space complexity, i.e., the memory required to store the intermediate results during the solving process [35].

For most applications, like water harvesting, weather forecasting, or optimization processes, where the DPT estimation involves iterative calculations, complexity can be significant beyond just the number of operations. Complex equations with many variables or nested operations may require more calculations and memory to store intermediate results, increasing both time and space complexity. However, reducing the number of variables can simplify implementation and improve accessibility without substantially affecting computational efficiency.

The primary advantage lies in making the model easier to understand and apply, rather than in dramatically lowering computational requirements. Therefore, the objective is to find a model that, despite considering fewer parameters, yields results with minimal error and maintains practical usability.

Given the aforementioned premises, certain considerations must be taken into account. Determining the dew point for given ambient temperature and relative humidity involves a minimum of two variables. Although psychrometric charts are typically used to obtain the dew point, the process based on these two variables is manual. Reducing computational cost impels simplifying the complexity of the mathematical operations used. Therefore, the use of polynomial equations is justified as an optimal method for approximation and reduction of computational cost, considering the inherent complexity of the equations relevant in this context. Based on this, the subsequent variables are adopted:

- X: Ambient temperature,
- Y: Relative humidity,
- Z: Dew point temperature.

Defining the background to consider, it is also necessary to include the relevant boundary conditions. Understanding the relationship between temperature and relative humidity in atmospheric conditions is crucial for explaining water condensation. The psychrometric chart is a key tool in this regard, providing important insights. Specifically, the horizontal line at 0 °C on the chart, shown in Figure 2, marks the acceptable range where temperature and relative humidity intersect within feasible limits.

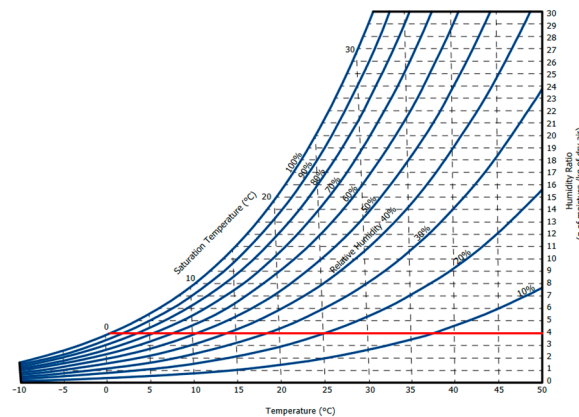


Figure 2. Psychrometric chart [36].

To ensure scientific accuracy, it is important to note that points below this line on the chart can be disregarded, as they do not significantly contribute to the analysis. This helps to minimize irrelevant factors and unnecessary complexity, resulting in a more precise dataset needed to develop a new equation.

The delineation of the horizontal line at 0 °C on the psychrometric chart corresponds to a specific relationship between temperature and relative humidity. This line, which marks the boundary of permissible atmospheric conditions for water condensation, can be defined as RH_{Min} using the equation:

$$RH_{Min} \geq 130.31 \cdot e^{(-0.061 \cdot T)} \tag{4}$$

where:

- RH represents relative humidity,
- T denotes temperature in degrees Celsius,
- e is Euler’s number.

This equation encapsulates the empirical relationship between temperature and relative humidity along the 0 °C line, defining that RH should not be less than RH_{Min} . By plotting this equation, it is possible to visually represent the range of temperature and relative humidity values where condensation of water vapor occurs under atmospheric conditions, as shown in Figure 3.

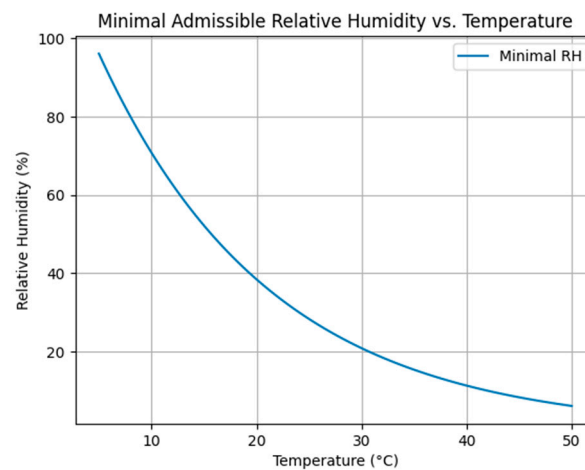


Figure 3. Minimal admissible relative humidity (RH_{Min}) for each T.

Finally, the mathematical process employed to derive the first- and second-degree equations from ambient temperature, relative humidity, and DPT data involves polynomial regression and least squares methods.

Due to limitations in available meteorological data, where direct dew point measurements are often unavailable and data are typically limited to parameters such as temperature and relative humidity, it was necessary to generate a custom dataset. This dataset was created to ensure consistency and cover a broad range of conditions for accurately modeling dew point temperature (DPT). By applying the Magnus–Tetens equation across defined ranges of ambient temperature (T) and relative humidity (RH), this study aimed to establish a comprehensive, reliable foundation for developing predictive models. Specifically, temperature values from 10 °C to 50 °C were paired with relative humidity values from 10% to 100%, using a resolution of 100 intervals for each parameter. This structured dataset provided the unique combinations needed to accurately calculate DPT values, addressing limitations and ensuring a consistent basis for model training and evaluation.

2.3.2. Derivation of the First-Degree Equation

Data on ambient temperature, relative humidity, and DPT are gathered into vectors. Subsequently, a matrix A is utilized to represent the variables X and Y along with a constant term. The coefficients a , b , and c of the Equation (1) are then computed through the least squares' method using the matrix inverse.

$$Z = aX + bY + c \quad (5)$$

2.3.3. Derivation of the Second-Degree Equation

Similarly, an A matrix with columns $X^2, X, Y^2, Y, 1$ is used to adjust a quadratic equation as:

$$Z = aX^2 + bX + cY^2 + dY + e \quad (6)$$

Both resulting Equations, (5) and (6), are mathematical expressions modeling the relation between the income variables (ambient temperature and relative humidity) and the outcome variable (dew point).

For the first-degree equation, the following expression is used:

$$A = [X \quad Y \quad 1] \quad (7)$$

For the second-degree equation, the expression defined by Equation (8) is used:

$$A = [X^2 \quad X \quad Y^2 \quad Y \quad 1] \quad (8)$$

To obtain the coefficients, Equation (9) is used:

$$\left(A^T \cdot A\right)^{-1} \cdot A^T \cdot Z = 0 \quad (9)$$

where:

- A^T is the transposed matrix of A ,
- $\left(A^T \cdot A\right)^{-1}$ is the inverse matrix of $\left(A^T \cdot A\right)$,
- Z is the coefficients vector.

Equations are obtained through fitting, then, a parametric optimization process is performed.

2.4. Optimization

2.4.1. Model Definition

The parametric mathematical model $f(x; \theta)$ describes the relationship between an independent variable x and a dependent variable y . This model contains parameters θ that need to be adjusted. In our case, $f(X, Y; a, b, c, d, e)$ represents the equation Z1 that we aim to adjust.

2.4.2. Observed Data

Observed data y_i correspond to values of the dependent variable at specific points x_i . In this case, the observed data are Zr obtained from the equation $Z(X, Y)$.

2.4.3. Objective Function

The objective function is the summation of the squares of the differences between the observed data and the values predicted by the model. This function is denoted as $J(\theta)$ and is defined according to Equation (10), which in our case would be the sum of the squares of the differences between Zr and Z1.

$$J(\theta) = \sum_{i=1}^n [y_i - f(x_i; \theta)]^2 \quad (10)$$

2.4.4. Optimization Model

The objective is to find the values of the parameters θ that minimize $J(\theta)$. This can be achieved by solving the system of equations given by the partial derivatives of J with respect to each parameter, setting them to zero as described in Equation (11) [37–39].

$$\frac{\partial J}{\partial \theta_j} = -2 \cdot \sum_{i=1}^n [y_i - f(x_i; \theta)] \frac{\partial f(x_i; \theta)}{\partial \theta_j} = 0 \quad (11)$$

These equations can be numerically solved using methods such as the Levenberg–Marquardt Method (LMM), which combines gradient descent techniques and the Gauss–Newton method to find optimal parameter values [40].

In this case, the LMM is employed for numerical optimization. It is an iterative algorithm for solving non-linear least squares problems. The LMM merges the advantages of the gradient descent method and the Gauss–Newton method. The algorithm iteratively adjusts the parameters of the function to minimize the cost function, which, in this case, is the sum of the squares of the differences between the observed and predicted values. The key to apply the LMM is to adjust the magnitude of the parameter update to strike a balance between the convergence speed of the Gauss–Newton method and the robustness of the gradient descent method. In mathematical terms, the Levenberg–Marquardt algorithm adjusts the parameters as described in Equation (12):

$$\theta_{new} = \theta_{current} - \left(J^T \cdot J + \lambda I\right)^{-1} \cdot J^T \cdot r \quad (12)$$

where:

- θ_{new} are the new parameters to calculate,
- $\theta_{current}$ are the current parameters,
- J is the Jacobian matrix,
- r corresponds to the residual vector (difference between the observed and the predicted values),
- λ is a regularization parameter.

The parameter λ is adjusted during the iterations to control the convergence of the method. If λ is small, the method resembles the Gauss–Newton method, and if it is large, it resembles the gradient descent method. This dynamic adjustment helps to deal with convergence and robustness issues at different stages of the optimization process.

2.4.5. Optimal Solution

Once the optimal values of the parameters θ are found, the adjusted model $f(x; \theta_{optimal}) = Z1$ is obtained, fitted to the observed data Zr . This process aims to minimize the discrepancy between the model and the observed data, favouring a better representation of the underlying phenomenon described by the model.

2.5. Perform Evaluation

Statistical parameters allow assessing the level of confidence and reliability of the estimates of the model. The performance of the empirical equations modeled is evaluated using R^2 , RMSE, MSE, and MAE indices.

The Coefficient of Determination (R^2) measures the proportion of the variability in the dependent variable that is explained by the independent variable(s) in the model. RMSE provides an estimate of the average magnitude of the errors between estimated and observed values. Similar to RMSE, MSE is commonly used in optimization problems and is sensitive to large errors. MAE measures the average absolute errors, providing a more interpretable scale than MSE. Finally, STD is widely used as a measure of variability or dispersion.

In addition to the accuracy evaluation, it is necessary to study the computational cost of the equations in terms of time and memory, and these equations are tested with various input sizes using different values. Execution time is recorded, and memory usage is tracked to measure peak memory consumption.

3. Results

The following section presents the outcomes of the analysis, emphasizing the first- and second-degree equations obtained via the optimization procedure. Quantitative results, inclusive of statistical analyses and graphical comparisons, are provided. Specifically, the equations are plotted alongside the observed data, and the error rates between these equations and the reference equation against the observed data are depicted. Furthermore, the statistical error rates are presented to offer further insight into the performance and accuracy of the derived models. This thorough examination aims to offer insights into the efficacy and reliability of the derived equations in describing the underlying phenomena. Table 1 presents the mathematical expressions of both obtained equations, and Figure 4 represents the surface defined by each equation. Figure 4a shows the dataset (red points) against the planar surface of the first-degree equation (blue surface). Likewise, Figure 4b, represents the dataset (red points) against the surface generated by the second-degree equation (blue surface).

Table 1. Equations obtained.

Equation	Non-Optimized	Optimized
1st Degree	$0.9063 \cdot X + 0.3458 \cdot Y - 28.1317$	$0.8912 \cdot X + 0.3595 \cdot Y - 27.9842$
2nd Degree	$-0.00037 \cdot X^2 + 1.2175 \cdot X - 0.0035 \cdot Y^2 + 0.7474 \cdot Y - 43.8711$	$-0.00013 \cdot X^2 + 0.93 \cdot X - 0.003 \cdot Y^2 + 0.66 \cdot Y - 35.39$

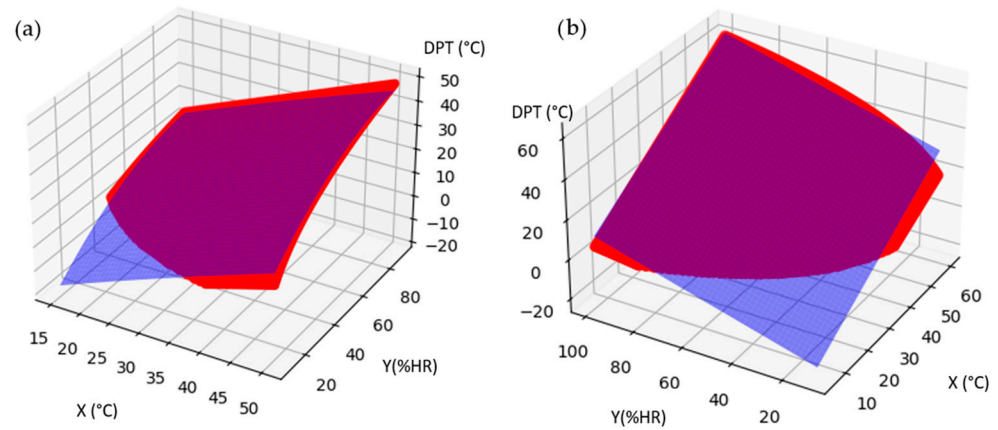


Figure 4. Surface representation of the defined equations (blue) and dataset (red). (a) 1st degree equation; (b) 2nd degree equation.

Reaching the DPT is unfeasible under conditions falling below the delineated threshold, as depicted by the red line in Figure 2. Additionally, the practical limitations of commercial cooling systems render temperatures below approximately 5–7 °C [41,42] unattainable, further constraining the applicability of predictive models in real-world scenarios. To address this, adjustments were made to the Magnus–Tetens’ equation to preclude erroneous values below 0 °C. Furthermore, empirical data revealed that relative humidity rates of 20% become feasible only upon attaining temperatures exceeding 25 °C. Consequently, the observed dataset was restricted to relative humidity rates surpassing this threshold to optimize the utility of available data points. Notably, this study scrutinized approximately 9000 data points encompassing temperatures ranging from 5 to 50 °C and relative humidity spanning from 20 to 100%, with each parameter measured at 300 intervals between the minimum and maximum values. To calibrate and validate predictive models like the second-order polynomial, a large dataset is crucial. While, theoretically, only a few points are required to fit a polynomial, these would not suffice to ensure the model’s robustness, accuracy, and reliability across a wide range of conditions. The extensive dataset of 9000 points allows for capturing the inherent variability in the observed phenomena, thereby refining the model to generalize well to unseen data. This comprehensive approach ensures that the model not only fits the given data accurately, but also performs reliably under various conditions, preventing overfitting and improving predictive capabilities. In essence, the large dataset serves to enhance the model’s validity and utility, making the predictions more trustworthy and applicable in real-world scenarios.

Figure 5 illustrates the error rates of each equation relative to the observed values, providing both 2D and 3D perspectives. The 3D plots represent a surface, encompassing regions beyond the specified boundaries, creating a waterfall-like visualization near the limits. Dark blue shades denote lower error values, indicative of temperatures below 0 °C, while yellow hues signify higher errors, associated with temperatures above 0 °C. Conversely, the 2D representations employ a contour plot method to present a heatmap of error distribution across temperature and relative humidity ranges.

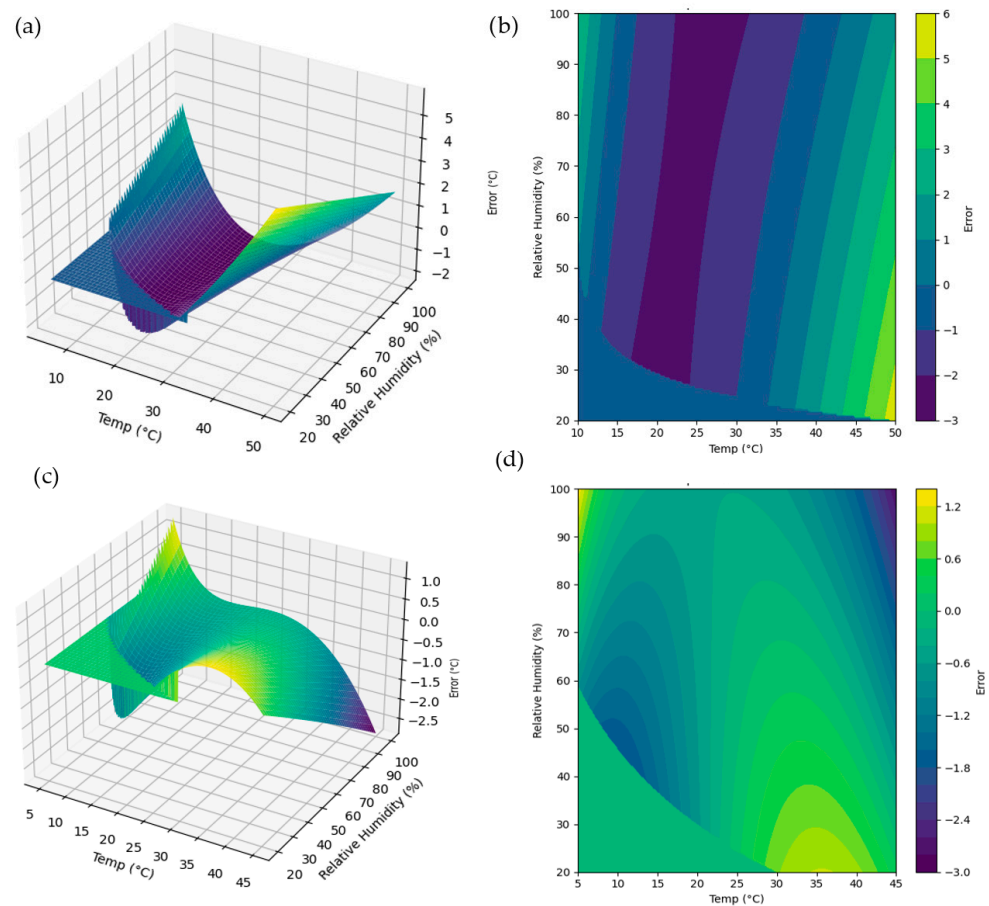


Figure 5. Error rate of the 1st and 2nd Degree Eqs. vs. Observed data. (a) 1st D.E. 3D representation. (b) 1st D.E. Planar representation. (c) 2nd D.E. 3D representation. (d) 2nd D.E. Planar representation.

The obtained first-degree equation produces a parabolic distribution of the errors, with maximum values up to 6 °C over the observed values, while underestimations reach 3 °C under observed values. The 3D surface plot in Figure 5a shows significant variances with pronounced peaks and troughs, highlighting extensive underestimations under high temperature and mid to low humidity, and overestimations under cooler, highly humid conditions. The 2D heatmap, Figure 5b, clearly illustrates the errors with vertical gradients that show increasing error magnitudes with rising temperatures across nearly all humidity levels, confirming the tendency of the equation to overestimate dew point in warmer conditions.

The obtained second-degree equation produces a non-homogeneous distribution of the errors, with maximum values up to 1.2 °C over the observed values, while underestimations reach a difference of 3 °C under observed values. Figure 5c shows that underestimation errors are more pronounced in conditions of high temperature and low humidity, which is evident in the deeper areas of the graph. Conversely, the equation demonstrates greater precision under conditions of high relative humidity, as indicated by lower elevations on the Z-axis. Additionally, slight overestimations are noted in conditions of intermediate temperature and high humidity. It is important to highlight that the values in the lower left corner, which show a value of zero, are excluded from the analysis due to being outside the established boundary conditions. This exclusion is relevant, as these values do not contribute to the analysis. Figure 5d displays a flat representation of the surface shown in Figure 5c as a heat map for a more generalized view. The performance across a broad range of environmental conditions is robust. Specifically, in conditions of high relative humidity, close to 100%, and across all temperature ranges, the equation exhibits remarkable precision, reflected by the more neutral colors in the visualization.

Figure 6 shows the graphical representations of the error rate obtained using the Thumb equation as a representative example of a commonly used equation for estimating DPT from ambient temperature and relative humidity. The results highlight substantial errors. Specifically, the 3D surface plot from Figure 6a displays a significant underestimation of dew point at lower temperatures, increasing together with the relative humidity. Conversely, at higher temperatures, it produces homogeneous accurate results independently from the relative humidity. In the case of the 2D heatmap in Figure 6b, it provides a detailed visualization of these discrepancies across the temperature and humidity spectrum. The error magnitude increases markedly with temperature, peaking particularly in the higher temperature ranges, where errors escalate to over 12 units. This gradient shift from cool to warm hues in the heatmap clearly illustrates how the error magnitude is exacerbated by increasing temperatures, regardless of humidity levels.

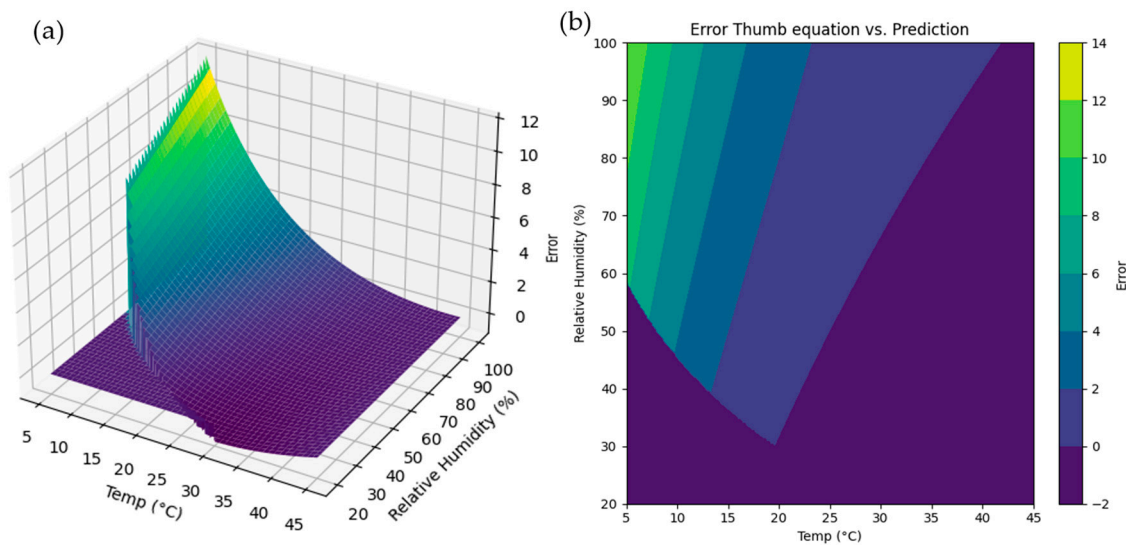


Figure 6. Absolute error rate of the Thumb Eq. vs. Observed data. (a) 3D representation. (b) Planar representation.

This analysis reveals that the traditionally used model has limited efficacy under varying climatic conditions, particularly failing to provide reliable predictions at higher temperatures.

Following the graphical presentations, an analysis of statistical parameters is conducted. This analysis, which results are shown in Table 2, includes R-squared (R^2), Root Mean Squared Error (RMSE), Mean Squared Error (MSE), Mean Absolute Error (MAE), and Standard Deviation. These metrics play a pivotal role in evaluating the accuracy and performance of the models, providing insights into the degree of variation between predicted and observed values. Their examination enables a comprehensive understanding of the efficacy of the predictive equations.

Table 2. Error indices.

	1st Degree Eq	2nd Degree Eq	Rule of Thumb
R^2	0.98	1	0.95
RMSE	1.82	0.71	2.67
MSE	3.33	0.51	7.13
MAE	1.44	0.53	1.45
STD	1.82	0.62	2.39
Max Error *	4.88	2.92	12.95
Mean Error *	1.59	0.72	1.805

* After 10,000 random calculations.

The statistical parameters provided for the three equations reveal some interesting insights into their performance. The second-degree equation stands out distinctly, achieving a perfect R-squared value of 1.00, which suggests it perfectly captures the variance in the dependent variable from the predictors. It also records the lowest errors across RMSE, MSE, and MAE, indicating its high accuracy and reliability in prediction. On the other hand, while the first-degree and Thumb equations also exhibit relatively high R-squared values, they fall short on error metrics, with the Thumb equation notably showing the highest errors and thus the least precision. This divergence in performance highlights the superior capability of the second-degree equation in providing reliable and accurate predictions under the conditions tested, while also underscoring the limitations of the more traditionally used Thumb equation in terms of accuracy and consistency.

In addition to the accuracy evaluation, it is necessary to study the computational cost of the four equations in terms of time and memory, and these equations are tested with various input sizes (10, 100, 500, 1000, 5000, 10,000, 12,000, 14,000, and 19,000) using random values within the range of 0 to 100. The test is conducted on the Google Colab cloud platform, utilizing a system with 12.67 GB of RAM and two cores of an AMD EPYC 7B12 processor running at 2.25 GHz (AMD, Santa Clara, CA, USA). Execution time is recorded, and memory usage is tracked to measure peak memory consumption. For each input size, random values of temperature and relative humidity are generated, and a mesh grid is created. The execution time and memory usage for each equation are then measured and recorded. Table 3 and Figure 7 capture this test and show the results. In Figure 7 it is possible to observe that for the Magnus–Tetens’ equation, for inputs larger than 13,500 iterations, the graphic turns horizontal; this is due to the impossibility to run this simulation because of RAM restrictions.

Table 3. Time and memory usage required by each equation according to different input size sets.

Input Size	Rule of Thumb		1st Degree Eq		2nd Degree Eq		Magnus–Tetens_Eq	
	Time (s)	Memory (MB)	Time (s)	Memory (MB)	Time (s)	Memory (MB)	Time (s)	Memory (MB)
10	0.101348	0.000	0.101430	0.000	0.100395	0.000	0.100561	0.000
100	0.100687	0.289	0.100642	0.000	0.100640	0.000	0.100902	0.257
500	0.109729	2.339	0.104308	3.089	0.105810	3.605	0.119401	5.722
1000	0.111176	4.042	0.111405	15.066	0.118247	15.066	0.144974	22.886
5000	0.343232	175.566	0.321507	190.738	0.542450	190.738	1.018584	190.738
10,000	0.675680	1525.887	0.734755	1525.891	1.722551	1525.953	3.547877	3814.711
12,000	0.797302	2197.273	0.867124	2197.293	2.032610	2197.326	4.186645	5493.221
13,500	0.925682	2990.741	1.010614	2990.786	2.359895	2990.778	4.860767	7476.830
19,000	1.290548	5508.481	1.403382	5508.478	3.290072	5508.479	-	-

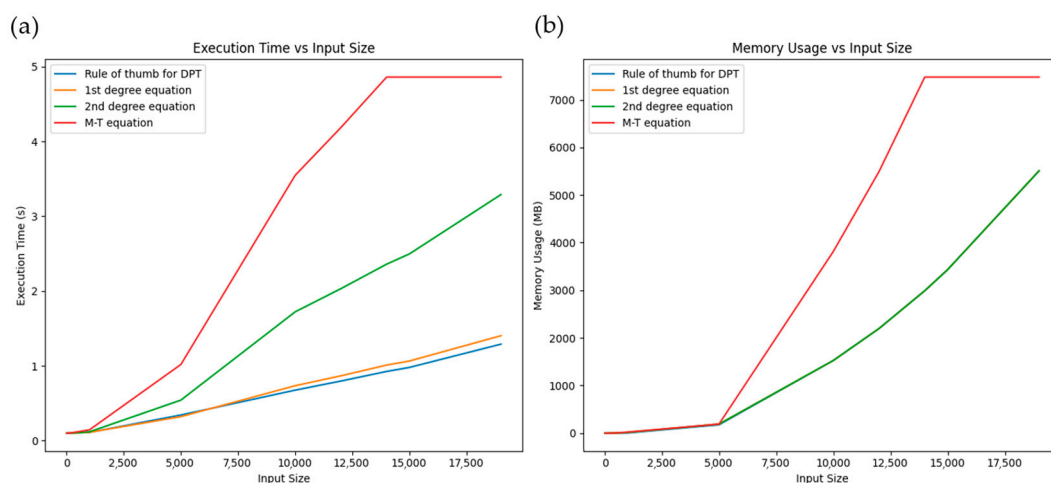


Figure 7. Computational cost results allowing RAM usage. (a) Execution time versus input size. (b) Memory usage versus input size.

Additionally, equations were tested with the same methodology, replacing the use of RAM for writing intermediate results to a file, as represented in Figure 8. Firstly, data and results are stored one by one (Figure 8a,b), and secondly, in blocks of 1000 entries (Figure 8c,d). The execution time and memory usage for each equation were measured and recorded, ensuring efficient memory management. Figure 8 illustrates the execution time, in the first case, Figure 8a, and in the second case, Figure 8c. Additionally, the memory usage across iterations is shown for the first case in Figure 8b and for the second case in Figure 8d, highlighting the performance differences between the equations. Figure 8a,c displays the averaging of each 100 results to enhance clarity and avoid noise.

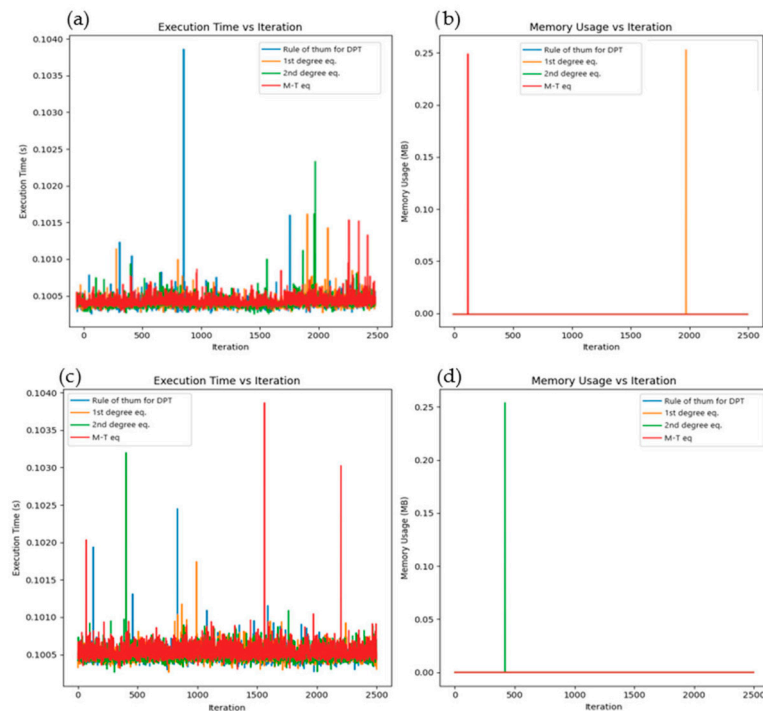


Figure 8. Execution Time and Memory usage vs. Iteration. (a) Execution time for results stored one by one; (b) memory usage for results stored one by one; (c) execution time for results stored in sets of 100 iterations; (d) memory usage for results stored in sets of 100 iterations.

In the case of RAM usage limitations, the results show a much slower individual behavior. Despite individual and sporadic peaks, they do not represent a significant variance (around 1% over the standard results); likewise in the case of RAM, where just sporadic peaks appear.

4. Discussion

This study evaluated two models designed to estimate DPT from ambient temperature and relative humidity. The performance of each model was analyzed through statistical parameters and error distribution. Considering the statistical parameters, the R-squared (R^2) values range over 0.95 in all cases, with the proposed second-degree equation achieving a perfect score of 1.00, indicating that it captures all the variance in the dependent variable from the predictors. The RMSE and MSE both highlight the second-degree equation as the most accurate, showing the smallest errors among the three compared equations, while the Thumb equation exhibits the highest errors, suggesting it is the least precise. The MAE confirms this pattern, with the second-degree equation again showing the lowest error, indicative of predictions that are closest to the observations. Lastly, the STD of the errors also confirms this trend, with the second-degree equation showing the least variability in its predictions. Overall, the second-degree equation outperforms the other two across all considered metrics, making it the most reliable and accurate for practical applications,

while the Thumb equation, despite having a decent R-squared value, proves less reliable due to its higher error rates and greater estimation variability.

The error distributions highlight the relative performance of the equations across varied environmental conditions. It is possible to observe that while the second-degree equation maintained a consistent accuracy across a wide range of temperatures and humidities, the first-degree equation struggled, particularly under extreme conditions. The same problem was observed in the Thumb equation under low temperature conditions. This variance in performance underscores the importance of choosing a model that robustly handles the complex interactions between multiple atmospheric variables.

Furthermore, these findings suggest that models relying on a linear structure, like the Thumb and first-degree equations, may not fully account for the non-linear interactions between temperature and relative humidity under extreme conditions. By contrast, the second-degree equation, with its quadratic components, is inherently better equipped to capture such complexities, enhancing its reliability for applications where fluctuations in environmental conditions are prevalent.

This study's results highlighted several factors influencing model accuracy, including the complexity of the model, the quality and range of the dataset, and the mathematical robustness of the modeling process. The iterative approach adopted in this study, involving repeated refinement and validation of the models, helped simplify the final equations, providing shorter and more user-friendly coefficients. This process was crucial in ensuring that the models remained adaptable and accurate over diverse testing scenarios.

The analysis of the results of computational cost reveals important insights into the efficiency of the equations under different input sizes. Focusing on execution time, the rule of thumb and 1st degree equation exhibit the fastest computation times across all tested sizes. Their simplicity in terms of arithmetic operations contributes to their efficiency. The 2nd degree equation shows a moderate increase in execution time, particularly for larger input sizes. This can be attributed to the quadratic terms, which require more computational resources, while the Magnus–Teten equation is the slowest among all the tested equations, with a significant increase in execution time for larger inputs. This is expected due to the logarithmic and multiple division operations involved.

Regarding memory usage, the rule of thumb and the 1st and 2nd degree equations show relatively similar results, especially for larger input sizes. This similarity may primarily be due to the large and consistent input and output array sizes. In a different way, the Magnus–Teten equation stands out with substantially higher memory usage, especially for the largest input size. The complex mathematical operations, including logarithms, likely contribute to this increased memory requirement. Furthermore, the results, shown in the figures, indicate that while using RAM for storing intermediate results provides the fastest access, alternative methods such as writing results to provisional files can introduce significant overhead, increasing the computation time due to slower disk I/O operations.

Given the substantial memory usage observed with the Magnus–Tetens equation, the developed second-degree model demonstrates a significant advantage, maintaining efficiency without compromising accuracy. This makes it a feasible alternative in systems with constrained memory resources, where the Magnus–Tetens equation may not be sustainable, particularly for high-frequency data streams or real-time applications.

Although the Thumb equation is widely used because it provides very good results with minimal errors at high temperatures, its performance is poor at low temperatures, regardless of the relative humidity ratio. This is problematic because accurate dew point modeling is critical at low temperatures, where the margin for error is smaller. In applications such as water harvesting, the dew point directly influences available production, and in other applications, it indirectly affects the energy consumption of the process.

The second-degree equation presents more generally reliable results because it maintains high accuracy and low error rates across a wider range of temperatures and humidity conditions. It is able to represent complex relationships between temperature and humidity more effectively than simpler models. This consistency is particularly important in practical

applications where varying environmental conditions can significantly impact performance. The comprehensive validation process and iterative refinement of the second-degree equation also contribute to its reliability, making it a suitable choice for accurate and dependable dew point modeling.

Furthermore, these findings imply that in conditions requiring high precision, such as low-temperature scenarios in meteorological and industrial applications, the second-degree equation may offer critical advantages. Given its demonstrated accuracy and robustness, it stands out as a viable alternative for operational systems that require consistent performance across a diverse range of conditions, supporting a broad array of applications, including energy-efficient building climate control and agricultural monitoring systems.

5. Conclusions

This study has developed and assessed a model for estimating dew point temperature (DPT), a crucial factor for thermal and energy applications. The new equation, obtained through non-linear regression fitting and parametric optimization, uses only ambient temperature and relative humidity, simplifying input requirements while maintaining high accuracy. Validated through extensive data comparison, it demonstrates consistent accuracy under real environmental conditions, ensuring reliable performance in critical applications.

First-degree and a second-degree polynomial equations were modeled and compared together and against the commonly used rule of thumb equation for dew point. The findings demonstrate that the obtained second-degree equation provides significantly better predictions than the commonly used Thumb rule and the first-degree equation. Specifically, the second-degree equation achieved an R^2 value of 1, RMSE of 0.71, and a standard deviation of 0.62, highlighting its potential for reliable and precise estimations. The precision and reliability of the second-degree equation make it particularly useful for practical applications, including weather forecasting, water harvesting, thermal comfort in buildings, heat recovery systems, and humidity control in agricultural settings. The first-degree equation also showed good performance (R^2 equal to 0.98, RMSE of 1.82, STD of 1.82), surpassing the Thumb rule (R^2 equal to 0.95, RMSE of 2.67, STD of 2.39) in accuracy, which indicates that even simpler models can be effective.

A notable advantage of the developed equations lies in their efficient memory usage, which remains stable and manageable even with large datasets, unlike the Magnus–Tetens equation, which exhibits high and exponentially increasing memory demands. The developed equations use 2.5 times less RAM than the Magnus–Tetens, enabling them to process large datasets more feasibly for real-time applications such as weather monitoring and industrial humidity control. The first-degree equation matches the Thumb rule in execution time, while the second-degree equation requires only half the processing time of the Magnus–Tetens, providing both memory and time efficiency. Furthermore, the simplicity of these equations makes them far easier to implement and integrate into various systems compared to complex ML models, which are often computationally intensive and act as “black boxes.” In contrast, the developed equations offer transparent and interpretable relationships between temperature, humidity, and dew point, eliminating the need for specialized recalibration. These characteristics make them robust, scalable, and well-suited for practical applications, addressing the complexity of traditional empirical models and the opacity of ML approaches.

This equation is particularly useful for environmental studies that utilize GIS-based tools (e.g., PVGIS), which provide localized atmospheric data with a limited number of parameters. Having a model dependent on as few parameters as possible is crucial for its applicability and real-world implementation. For instance, in water harvesting from ambient air at various locations, this equation can accurately model and estimate potential water production, making it a helpful, reliable, and user-friendly tool for practical applications.

Author Contributions: Conceptualization, J.A.H.-T. and A.B. (Andrea Baccioli); methodology, J.A.H.-T., J.P.T., A.B. (Aldo Bischi), and A.B. (Andrea Baccioli); software, J.A.H.-T., R.S.-H. and A.B. (Aldo Bischi); validation, R.S.-H. and A.B. (Aldo Bischi); formal analysis, J.A.H.-T., A.B. (Aldo Bischi), and A.B. (Andrea

Baccioli); investigation, J.A.H.-T., A.B. (Aldo Bischi), and A.B. (Andrea Baccioli); resources, R.S.-H. and J.P.T.; data curation, J.A.H.-T., R.S.-H. and A.B. (Aldo Bischi); writing—original draft preparation, J.A.H.-T.; writing—review and editing, J.P.T., A.B. (Andrea Baccioli), and A.B. (Aldo Bischi); visualization, J.A.H.-T., R.S.-H. and A.B. (Aldo Bischi); supervision, J.P.T., A.B. (Aldo Bischi), and A.B. (Andrea Baccioli); project administration, J.P.T. and R.S.-H.; funding acquisition, J.P.T. All authors have read and agreed to the published version of the manuscript.

Funding: This work was supported by the project entitled “Renewable energies for Africa: Effective valorization of agri-food wastes (REFFECT AFRICA)”. This project has received funding from the European Union’s Horizon 2020 Research and Innovation programme under the Grant Agreement number 101036900.

Institutional Review Board Statement: Not applicable.

Informed Consent Statement: Not applicable.

Data Availability Statement: Publicly available datasets were analyzed in this study. This data can be found in: https://github.com/JoseAUHU/Dataset_Dew_Point.

Conflicts of Interest: The authors declare no conflicts of interest.

References

1. Yan, J.; Huang, J. Modeling Method of Dew-Point Temperature Prediction in Industrial Workshop Based on Machine Learning. In Proceedings of the IEEE 5th Conference on Energy Internet and Energy System Integration (EI2), Taiyuan, China, 22–24 October 2021; IEEE: Piscataway, NJ, USA, 2021; pp. 3160–3165.
2. Jarimi, H.; Powell, R.; Riffat, S. Review of sustainable methods for atmospheric water harvesting. *Int. J. Low-Carbon Technol.* **2020**, *15*, 253–276. [[CrossRef](#)]
3. Deka, P.C.; Patil, A.P.; Kumar, P.Y.; Naganna, S.R. Estimation of dew point temperature using SVM and ELM for humid and semi-arid regions of India. *ISH J. Hydraul. Eng.* **2018**, *24*, 190–197. [[CrossRef](#)]
4. Lawrence, M.G. The relationship between relative humidity and the dewpoint temperature in moist air: A simple conversion and applications. *Bull. Am. Meteorol. Soc.* **2005**, *86*, 225–234. [[CrossRef](#)]
5. Hill, A.J.; Dawson, T.E.; Shelef, O.; Rachmilevitch, S. The role of dew in Negev Desert plants. *Oecologia* **2015**, *178*, 317–327. [[CrossRef](#)]
6. Chung, C.H.; Chiang, Y.M.; Chang, F.J. A spatial neural fuzzy network for estimating pan evaporation at ungauged sites. *Hydrol. Earth Syst. Sci.* **2012**, *16*, 255–266. [[CrossRef](#)]
7. Lin, J.; Wang, R.; Li, C.; Wang, S.; Long, J.; Chua, K.J. Towards a thermodynamically favorable dew point evaporative cooler via optimization. *Energy Convers. Manag.* **2020**, *203*, 112224. [[CrossRef](#)]
8. Sarkar, M. A new theoretical formulation of dew point temperatures applicable for comfort air-cooling systems. *Energy Build.* **2015**, *86*, 243–256. [[CrossRef](#)]
9. Elbir, A.; Kodaloglu, A.F.; Ucgul, I. Thermodynamic analysis for industrial cabinet providing simultaneous heating and cooling that can be used in the food industry. *Therm. Sci.* **2022**, *26*, 2845–2854. [[CrossRef](#)]
10. Lin, J.; Thu, K.; Karthik, S.; Shahzad, M.W.; Wang, R.; Chua, K.J. Understanding the transient behavior of the dew point evaporative cooler from the first and second law of thermodynamics. *Energy Convers. Manag.* **2021**, *244*, 114471. [[CrossRef](#)]
11. Rao, A.K.; Fix, A.J.; Yang, Y.C.; Warsinger, D.M. Thermodynamic limits of atmospheric water harvesting. *Energy Environ. Sci.* **2022**, *15*, 4025–4037. [[CrossRef](#)]
12. Tsilingiris, P. Thermophysical and transport properties of humid air at temperature range between 0 and 100 °C. *Energy Convers. Manag.* **2008**, *49*, 1098–1110. [[CrossRef](#)]
13. Wang, Z.; Chen, H.; Weng, S. “Partial pressures” of humid air in wide pressure and temperature ranges. *Front. Energy* **2013**, *7*, 511–517. [[CrossRef](#)]
14. Lu, H.; Shi, W.; Guo, Y.; Guan, W.; Lei, C.; Yu, G. Materials engineering for atmospheric water harvesting: Progress and perspectives. *Adv. Mater.* **2022**, *34*, 2110079. [[CrossRef](#)]
15. Jakosky, B.M.; Farmer, C.B. The seasonal and global behavior of water vapor in the Mars atmosphere: Complete global results of the Viking atmospheric water detector experiment. *J. Geophys. Res. Solid Earth* **1982**, *87*, 2999–3019. [[CrossRef](#)]
16. Bahadori, A.; Mokhatab, S. Predicting water content of compressed air: This new correlation can be helpful when measured data is not available. *Chem. Eng.* **2008**, *115*, 56–58.
17. Yang, M. Air compressor efficiency in a Vietnamese enterprise. *Energy Policy* **2009**, *37*, 2327–2337. [[CrossRef](#)]
18. Heldman, D.R.; Moraru, C.I. *Encyclopedia of Agricultural, Food, and Biological Engineering*; CRC Press: Boca Raton, FL, USA, 2010.
19. Hubbard, K.; Mahmood, R.; Carlson, C. Estimating Daily Dew Point Temperature for the Northern Great Plains Using Maximum and Minimum Temperature. *Agron. J.* **2003**, *95*, 323–328. [[CrossRef](#)]
20. Kisi, O.; Kim, S.; Shiri, J. Estimation of dew point temperature using neuro-fuzzy and neural network techniques. *Theor. Appl. Climatol.* **2013**, *114*, 365–373. [[CrossRef](#)]

21. Mehdizadeh, S.; Mohammadi, B.; Ahmadi, F. Establishing coupled models for estimating daily dew point temperature using nature-inspired optimization algorithms. *Hydrology* **2022**, *9*, 9. [[CrossRef](#)]
22. Nazeri-Tahroudi, M.; Ramezani, Y. Estimation of dew point temperature in different climates of Iran using support vector regression. *J. Hung. Meteorol. Serv.* **2020**, *124*, 521–539. [[CrossRef](#)]
23. Baghban, A.; Bahadori, M.; Rozyn, J.; Lee, M.; Abbas, A.; Bahadori, A.; Rahimali, A. Estimation of air dew point temperature using computational intelligence schemes. *Appl. Therm. Eng.* **2016**, *93*, 1043–1052. [[CrossRef](#)]
24. Mehdizadeh, S.; Behmanesh, J.; Khalili, K. Application of gene expression programming to predict daily dew point temperature. *Appl. Therm. Eng.* **2017**, *112*, 1097–1107. [[CrossRef](#)]
25. Marques-Silva, J.; Ignatiev, A. No silver bullet: Interpretable ml models must be explained. *Front. Artif. Intell.* **2023**, *6*, 1128212. [[CrossRef](#)]
26. Haji-Savameri, M.; Menad, N.A.; Norouzi-Apourvari, S.; Hemmati-Sarapardeh, A. Modeling dew point pressure of gas condensate reservoirs: Comparison of hybrid soft computing approaches, correlations, and thermodynamic models. *J. Pet. Sci. Eng.* **2020**, *184*, 106558. [[CrossRef](#)]
27. Naganna, S.R.; Deka, P.C.; Ghorbani, M.A.; Biazar, S.M.; Al-Ansari, N.; Yaseen, Z.M. Dew point temperature estimation: Application of artificial intelligence model integrated with nature-inspired optimization algorithms. *Water* **2019**, *11*, 742. [[CrossRef](#)]
28. Dongarra, J.; Gates, M.; Haidar, A.; Kurzak, J.; Luszczek, P.; Tomov, S.; Yamazaki, I. Accelerating numerical dense linear algebra calculations with GPUs. In *Numerical Computations with GPUs*; Springer: Cham, Switzerland, 2014; pp. 3–28.
29. Demmel, J.; Hoemmen, M.; Mohiyuddin, M.; Yelick, K. Avoiding communication in sparse matrix computations. In Proceedings of the 2008 IEEE International Symposium on Parallel and Distributed Processing, Miami, FL, USA, 14–18 April 2008.
30. Asyabi, E.; Sharafzadeh, E.; SanaeeKohroudi, S.; Sharifi, M. CTS: An operating system CPU scheduler to mitigate tail latency for latency-sensitive multi-threaded applications. *J. Parallel Distrib. Comput.* **2019**, *133*, 232–243. [[CrossRef](#)]
31. Asensio, L.; Urraca, G.; Navarro, V. Consistency of Water Vapour Pressure and Specific Heat Capacity Values for Modelling Clay-Based Engineered Barriers. *Appl. Sci.* **2023**, *13*, 3361. [[CrossRef](#)]
32. Shao, X.; Deng, Q.; Jiang, M.; Chen, Q. Estimation of Water Vapor Density in Adiabatic Mixing of Cryogenic Gas and Moist Air. *Processes* **2022**, *10*, 2521. [[CrossRef](#)]
33. Peleg, N.; Fatchi, S.; Paschalis, A.; Molnar, P.; Burlando, P. An advanced stochastic weather generator for simulating 2-D high-resolution climate variables. *J. Adv. Model. Earth Syst.* **2017**, *9*, 1595–1627. [[CrossRef](#)]
34. Magomedov, M.N. On the accuracy of the Clausius-Clapeyron relation. *Vacuum* **2023**, *217*, 112494. [[CrossRef](#)]
35. Cormen, T.H.; Leiserson, C.E.; Rivest, R.L.; Stein, C. *Introduction to Algorithms*; MIT Press: Boston, MA, USA, 2009.
36. Meyer, D.; Thevenard, D. PsychroLib: A library of psychrometric functions to calculate thermodynamic properties of air. *J. Open Source Softw.* **2019**, *4*, 1137. [[CrossRef](#)]
37. Marquardt, D.W. An algorithm for least-squares estimation of nonlinear parameters. *J. Soc. Ind. Appl. Math.* **1963**, *11*, 431–441. [[CrossRef](#)]
38. Yan, Z.; Zhong, S.; Lin, L.; Cui, Z. Adaptive Levenberg–Marquardt algorithm: A new optimization strategy for Levenberg–Marquardt neural networks. *Mathematics* **2021**, *9*, 2176. [[CrossRef](#)]
39. Duc-Hung, L.; Cong-Kha, P.; Trang, N.T.T.; Tu, B.T. Parameter extraction and optimization using Levenberg-Marquardt algorithm. In Proceedings of the Fourth International Conference on Communications and Electronics (ICCE), Hue, Vietnam, 1–3 August 2012; IEEE: Piscataway, NJ, USA, 2012; pp. 434–437.
40. Gavin, H.P. *The Levenberg-Marquardt Algorithm for Nonlinear Least Squares Curve-Fitting Problems*; Department of Civil and Environmental Engineering, Duke University: Durham, NC, USA, 2022.
41. Lizarte, R.; Izquierdo, M.; Marcos, J.; Palacios, E. Experimental comparison of two solar-driven air-cooled LiBr/H₂O absorption chillers: Indirect versus direct air-cooled system. *Energy Build.* **2013**, *62*, 323–334. [[CrossRef](#)]
42. Pan, Q.; Peng, J.; Wang, R. Experimental study of an adsorption chiller for extra low temperature waste heat utilization. *Appl. Therm. Eng.* **2019**, *163*, 114341. [[CrossRef](#)]

Disclaimer/Publisher’s Note: The statements, opinions and data contained in all publications are solely those of the individual author(s) and contributor(s) and not of MDPI and/or the editor(s). MDPI and/or the editor(s) disclaim responsibility for any injury to people or property resulting from any ideas, methods, instructions or products referred to in the content.